Scattering from elongated objects: direct solution in $O(N \log^2 N)$ operations

E. Michielssen
A. Boag
W.C. Chew

Indexing terms: Algorithms, Electromagnetic wave scattering, Planewave scattering, Numerical analysis

Abstract: A recursive algorithm is presented for analysing TM and TE plane-wave scattering from two-dimensional elongated objects. The computational complexity and the memory requirements of the algorithm are $O(N \log^2 N)$ and $O(N \log N)$, respectively. The algorithm is based on the concept of a reduced representation and fast computation of fields that are radiated by quasialigned sources. While many existing fast algorithms for analysing electromagnetic scattering problems rely on iterative strategies, the proposed algorithm provides a direct solution to the scattering problem. The algorithm has a variety of potential applications, including the analysis of scattering from truncated and quasiperiodic structures, winglike structures, phased-array antennas and rough surfaces.

1 Introduction

Numerical algorithms for the analysis of electromagnetic scattering from elongated objects, i.e. structures whose dimensions extend primarily along one spatial axis and are uniform or of limited extent along the other two axes, are of great practical interest. A nonexhaustive list of potential applications includes the analysis of scattering from rough surfaces, winglike structures, truncated and quasiperiodic structures, as well as the radiation from large phased-array antennas (Fig. 1).

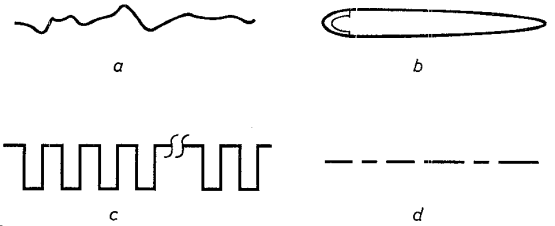

Fig. 1 *Examples of elongated structures that can be analysed using the proposed direct recursive algorithm*
a Rough surface, *b* Wing-like structure, *c* Truncated periodic structure, *d* Coplanar array

IEE Proceedings online no. 19960400

Paper first received 27th June 1995 and in revised form 30th January 1996

The authors are with the Department of Electrical & Computer Engineering, University of Illinois at Urbana–Champaign, Urbana, IL 61801, USA

The problem of scattering from an elongated object is readily formulated in terms of an electric field integral equation (EFIE), which can be subsequently discretised using the method of moments (MoM). Unfortunately, the direct solution of the MoM matrix equations becomes impractical as the electrical size of the object increases beyond a certain limit because of the $O(N^3)$ computational complexity of any direct solver. For large structures, iterative algorithms are sometimes useful alternatives to direct solvers. A number of fast algorithms that drastically accelerate the iterative solution of MoM matrix equations have recently been proposed. Examples include, but are not limited to, the fast multipole algorithm [1, 2], the impedance matrix localisation method [3, 4] and FFT-based methods [5, 6]. These fast algorithms make iterative methods an even more attractive alternative to direct solvers for large scatterers. Pak *et al.* and Tsang *et al.* [7–9] recently developed a class of fast iterative solvers, which are geared towards the analysis of scattering from rough surfaces. Unfortunately, with few exceptions, iterative solvers only consider one 'right-hand side' at a time, which makes them impractical when multiple excitations have to be analysed simultaneously.

To circumvent these problems, Chew and Lu [10] recently proposed a direct recursive algorithm for analysing scattering from a coplanar array of strips. Their algorithm has $O(N \log^2 N)$ computational complexity and $O(N \log N)$ memory requirements (Fig. 1*d*). These authors derive a plane-wave/spectral-domain representation of the two-dimensional (2D) Green's function and use this representation to recursively characterise the scattering from increasingly larger portions of the scatterer. Unfortunately, in its present form, this algorithm does not apply to nonplanar geometries, e.g. those of Fig. 1*a–c*.

In this paper, a novel fast recursive algorithm is presented for analysing TM and TE scattering from perfectly conducting and/or penetrable, arbitrarily shaped, but elongated objects. The proposed algorithm exhibits similarities to that of Chew and Lu [10]. However, the restriction of the latter algorithm, i.e. its nonapplicability to nonplanar structures, is lifted by abandoning the spectral/plane-wave representation of the 2D Green's function in favour of a reduced spatial representation of the fields that are scattered by an elongated object. This reduced spatial representation permits the computation of the fields radiated by N quasialigned sources, observed over an elongated domain that is aligned with the source domain, in terms of those radiated by $O(\log$

N) equivalent sources. The concept of a reduced field representation is directly related to that of the limited number of degrees of freedom that characterise electromagnetic fields [11–14], and permits the analysis of scattering by elongated, but nonplanar structures, without sacrificing the favourable computational complexity and memory requirements reported by Chew and Lu [10].

The purpose of the present paper is to introduce the proposed algorithm, to apply it to some simple grating structures, and to study its convergence properties. The application of the algorithm to rough surface scattering will be the topic of a future paper.

2 Formulation

In this Section, a recursive algorithm is presented for analysing TM scattering from elongated objects. Assume that the striplike, perfect electrically conducting (PEC) scatterer S, depicted in Fig. 2, is of length L and maximum height H with $H << L$, and is described by the equation $y^S = f(x^S)$. S is illuminated by an incident field $E_z^{inc}(\rho)$ (a time dependence $e^{j\omega t}$ is assumed and suppressed throughout this paper). No restrictions apply with respect to the nature of $E_z^{inc}(\rho)$, which could, for example, represent a plane wave or a Gaussian beam.

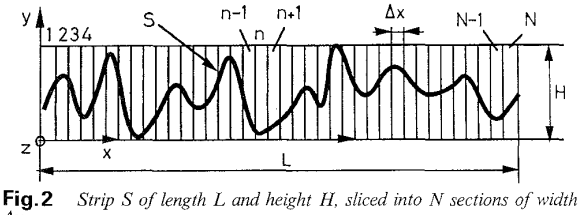

Fig. 2 *Strip S of length L and height H, sliced into N sections of width Δx*

The scattering from a strip is often analysed using the method of moments (MoM). An EFIE is constructed in terms of the z-directed current $J_z^S(\rho)$ residing on S. This EFIE enforces the total electric field along S to vanish:

$$E_z^{inc}(\rho) = -\int_S J_z^S(\rho')G(\rho,\rho')d\rho' \quad \forall \rho \in S \qquad (1)$$

Here, $G(\rho,\rho') = -\eta k/4H_0^{(2)}(k|\rho-\rho'|)$, η is the free-space impedance, $k = 2\pi/\lambda$ is the free-space wavelength), and $H_0^{(2)}(\cdot)$ denotes a zero-order Hankel function of the second kind. Next, S is subdivided into a large number, say N subsections, of width w_j, $j = 1, ..., N$, which are less than $\lambda/10$. It is assumed that the projected width of each subsection onto the x-axis is constant and is given by Δx (Fig. 2). A pulse basis function $p_j^S(\rho)$, representing a z-directed surface current, is associated with each subsection, and the total current on S is expressed in terms of a linear combination of these pulse functions as

$$J_z^S(\rho) = \sum_{j=1}^{N} I_j^S p_j^S(\rho) \qquad (2)$$

Substitution of eqn. 2 into eqn. 1 and enforcement of the resulting equation, at the centre ρ_i^S, $i = 1, ..., N$ of each of the subsections, results in an $N \times N$ system of linear equations in the expansion coefficients I_j^S. Solution of this system of equations permits the computation of related quantities, e.g. the strip's radar cross-section (RCS). The computational complexity of the direct solution of this system of equations is $O(N^3)$.

In contrast, the computational complexity of the proposed algorithm scales as $O(N \log^2 N)$ for fixed H and increasing L. The algorithm starts by considering a small portion S_1^- of S containing only its first subsection, starting from the left. S_1^+ denotes the remainder of the strip, composed of the $N - 1$ subsections to the right of S_1^-. The algorithm constructs the transition matrix [15] of S_1^-, which relates the amplitudes of the waves scattered by S_1^- to the amplitudes of all the waves that potentially illuminate S_1^-, i.e. $E_z^{inc}(\rho)$ and the field radiated by currents residing on S_1^+. Next, the algorithm iteratively considers increasingly larger substrips S_2^-, S_3^-, ..., S_N^- (S_n^- denotes that part of the S comprising subsections one through to n, and similarly, S_n^+ will denote subsections $n + 1$ through to N) and recursively constructs the corresponding transition matrices until the entire scatterer has been described. A brute-force implementation of such an algorithm results in a computational complexity of $O(N^3)$, because the transition matrices of arbitrarily shaped and excited objects contain $O(N^2)$ independent elements [15], and a recursive solution procedure requires updating this matrix N times. However, unlike a transition matrix describing an arbitrarily shaped object, the dimensions of the transition matrices describing elongated structures contain only $O(\log^2 N)$ independent elements. The fields scattered by an elongated object containing N sources can be represented in terms of those radiated by a reduced set of $O(\log N)$ carefully selected equivalent sources, which results in an algorithm with a computational complexity of $O(N \log^2 N)$.

The construction of these reduced sets of equivalent sources is the essence of the proposed algorithm and is discussed in Section 2.1. A recursive algorithm based on this reduced representation is described in Section 2.2. Section 2.3 focuses on computational complexity and the TE extension of the algorithm.

2.1 Reduced representation of radiated fields

This Section focuses on the construction of a reduced set of sources that is capable of representing the field that exists over an elongated domain due to sources residing on an elongated object oriented along the same direction.

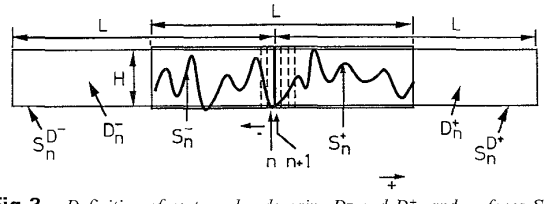

Fig. 3 *Definition of rectangular domains D_n^- and D_n^+, and surfaces S_n^{D-} and S_n^{D+} associated with S_n^- and S_n^+*
Pulse sources are indicated by dashes

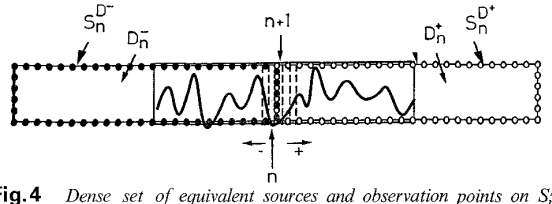

Fig. 4 *Dense set of equivalent sources and observation points on S_n^{D-} and S_n^{D+}*
Pulse sources are indicated by dashes

Throughout the remainder of this paper, we adopt the following notational convention: D_n^- and D_n^+, are

rectangular domains of dimensions $L \times H$ that contain S_n^- and S_n^+, respectively, as illustrated in Figs. 3–5. S_n^{D-} and S_n^{D+} denote the surfaces of D_n^- and D_n^+, respectively.

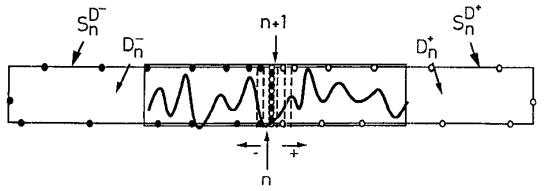

Fig. 5 *Corresponding reduced sets*
Pulse sources are indicated by dashes
● reduced set of source points
○ reduced set of observation points

The electric field scattered by S_n^- onto S_n^+ can be described in terms of the currents that reside on S_n^-, or, equivalently, in terms of the expansion coefficients I_j^S, $j = 1, ..., n$. Assuming that $n >> 1$, the possibility of describing this field in terms of a far smaller set of sources, in number proportional to $\log(L) \sim \log(N)$ will be shown. This equivalent set of sources for the current residing on S_n^- is constructed by invoking the uniqueness principle. The electromagnetic field radiated to the exterior of S_n^{D-} by an arbitrary current distribution $J_z^{S_n^-}(\rho)$ residing on S_n^- can always be represented in terms of the fields radiated by equivalent surface sources $J_{zn}^{SD^-}(\rho)$ residing on S_n^{D-}. Given $J_z^{S_n^-}(\rho)$, an integral equation can be constructed equating the fields due to $J_z^{S_n^-}(\rho)$ to those radiated by $J_{zn}^{SD^-}(\rho)$ just outside S_n^{D-}, and solved for $J_{zn}^{SD^-}(\rho)$. However, the present recursive algorithm does not call for an equivalent surface current $J_{zn}^{SD^-}(\rho)$ which regenerates the original field everywhere in space. Rather, for our purposes, it is sufficient that $J_{zn}^{SD^-}(\rho)$ reproduces the original fields radiated by $J_z^{S_n^-}(\rho)$ everywhere inside D_n^+. This can be accomplished by equating the fields radiated by $J_z^{S_n^-}(\rho)$ to those radiated by $J_{zn}^{SD^-}(\rho)$ on the surface S_n^{D+} bounding D_n^+. This leads to the following EFIE for $J_{zn}^{SD^-}(\rho)$:

$$\int_{S_n^-} J_z^{S_n^-}(\rho')G(\rho,\rho')ds' = \int_{S_n^{D-}} J_z^{S_n^{D^-}}(\rho')G(\rho,\rho')ds' \quad \forall\rho \text{ on } S_n^{D^+} \tag{3}$$

One might attempt to solve this EFIE using the MoM by expanding $J_{zn}^{SD^-}(\rho)$ in a set of pulse basis functions that span and reside on S_n^{D-} as

$$J_z^{S_n^{D^-}}(\rho) = \sum_{j=1}^{N^D} I_j^D p_j^{S_n^{D^-}}(\rho) \tag{4}$$

Let $\rho_{jn}^{SD^-}$, $j = 1, ..., N^D$ denote the centres of the pulses $p_{jn}^{SD^-}$. Enforcing eqn. 3 at the mirror images $\rho_{jn}^{SD^+}$, $j = 1, ..., N^D$ on S_n^{D+} of the $\rho_{jn}^{SD^-}$, results in a matrix equation of the form (Fig. 4)

$$\mathbf{V}^D = \overline{\mathbf{Z}}^D \mathbf{I}^D \tag{5}$$

where $\mathbf{V}^D = [V_i^D]$, $\overline{\mathbf{Z}}^D = [Z_{ij}^D]$, $\mathbf{I}^D = [I_j^D]$, $i, j = 1, ..., N^D$, and V_i and Z_{ij} are given by

$$\begin{aligned} Z_{ij}^D &= E(\rho_i^{S_n^{D^+}}, p_j^{S_n^{D^-}}) \\ V_i^D &= \sum_{m=1}^{n} I_m^S E(\rho_i^{S_n^{D^+}}, p_m^{S_n^-}) \end{aligned} \tag{6}$$

where

$$E(\rho,p) = \int G(\rho,\rho')p(\rho')d\rho' \tag{7}$$

Unfortunately, eqn. 5 does not provide a unique solution for the coefficient vector $\mathbf{I}^D$ because $\overline{\mathbf{Z}}^D$ is numerically rank deficient. The rank deficiency of $\overline{\mathbf{Z}}^D$ reflects the limited number of degrees of freedom N_{dof}, that characterise the fields in D_n^+ generated by an arbitrary distribution $J_{zn}^{SD^-}(\rho)$ of z-directed current sources residing on S_n^{D-} [12]. In other words, any field over D_n^+ due to an arbitrary current residing in D_n^- can be represented in terms of N_{dof} linearly independent components. N_{dof}, of course, depends on the desired accuracy in the field representation ε, and can be rigorously defined as

$$N_{dof} = \text{rank}(\overline{\mathbf{Z}}^D, \varepsilon) = \min\left\{\text{rank}(\overline{\mathbf{B}}) | \parallel \overline{\mathbf{Z}}^D - \overline{\mathbf{B}} \parallel < \varepsilon\right\} \tag{8}$$

N_{dof} can be computed by performing a singular value decomposition on $\overline{\mathbf{Z}}^D$, since N_{dof}, as defined by eqn. 8, is equal to the number of singular values larger or equal to ε [16]. A plot of the singular values of $\overline{\mathbf{Z}}^D$ reveals N_{dof} for a given accuracy ε in the field representation. Fig. 6 plots the singular values of $\overline{\mathbf{Z}}^D$ for $H = 0.5\lambda$ and L varying from 32λ to 2048λ, and demonstrates that, for fixed L, N_{dof} grows as $\log(1/\varepsilon)$. In other words, a significant drop in the tolerance level ε results in only a small increase in N_{dof} [12]. A detailed analysis of the data presented in Fig. 6 also shows that N_{dof} is proportional to $\log(L)$. Although the work of Chew and Lu [10] for the $H = 0$ case is based on a spectral-domain representation of Green functions, their analysis reveals a similar logarithmic dependence on L for the number of terms required in the Green function approximation. Hence, here we show that for $H \neq 0$ and $H << L$, the same asymptotic trend is still observed. This is because, for source and observation points far removed from the junction between D_n^- and D_n^+, the asymptotic behaviour of the Hankel function can still be approximated in terms of a logarithmic number of samples along the branch cut in its spectral representation [10]. The fact that, in this study, we use a spatial representation of the field instead of a spectral representation does, of course, not increase the information content of the field. Fig. 7 shows the dependence of N_{dof} on H for a fixed L by plotting the singular values of $\overline{\mathbf{Z}}^D$ for $L = 204.8\lambda_0$ and H varying from 0.3λ to 3.0λ. Analysis of the data presented in Fig. 7, for a fixed ε, reveals a linear dependence of N_{dof} on H ($<<L$).

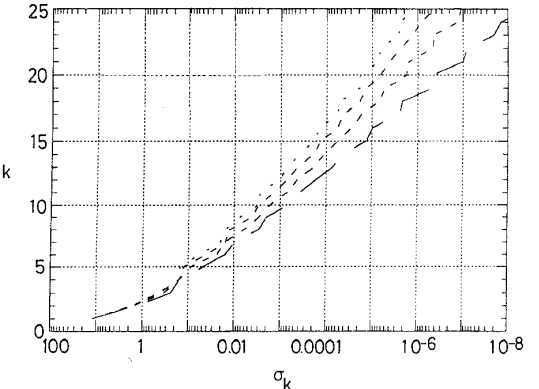

Fig. 6 *Singular values of the $\overline{\mathbf{Z}}^D$ matrix for $H = 1.5\ \lambda$ and various values of L*
All surfaces are sampled at a rate of $\lambda/10$
· · · · $L = 2048$
- - - - $L = 512$
– – – $L = 128$
——— $L = 32$

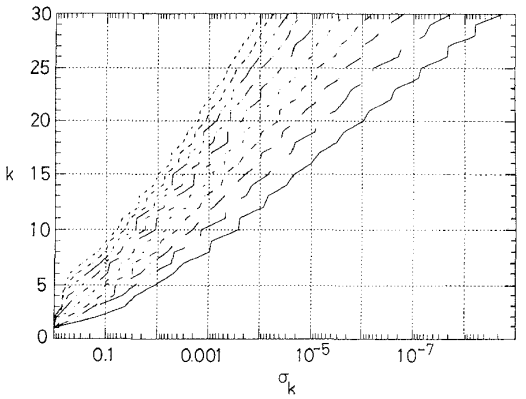

Fig. 7 *Singular values of the $\bar{\mathbf{Z}}^D$ matrix for $L = 204.8\ \lambda$ and various H*
- $H = 0.3$
- $H = 0.6$
- $H = 0.9$
- $H = 1.2$
- $H = 1.5$
- $H = 1.8$
- $H = 2.1$
- $H = 2.4$
- $H = 2.7$
- $H = 3.0$

The equivalent surface current could be computed as $\mathbf{I}^D = \bar{\mathbf{Z}}^{D\dagger}\mathbf{V}^D$, where † denotes a Moore–Penrose pseudoinverse [16]. However, more efficient field representations exist since the rank deficiency of $\bar{\mathbf{Z}}^D$ implies that its column range is spanned by the fields radiated by a small 'reduced set' of N_{dof} source pulses corresponding to the N_{dof} most linearly independent columns of $\bar{\mathbf{Z}}^D$. These columns can be identified by performing a rank-revealing QR (RRQR) decomposition with column pivoting on $\bar{\mathbf{Z}}^D$ [16–18]. The field radiated onto D_n^+ by any source in D_n^- can be represented in terms of the fields radiated by the sources corresponding to these columns. The locations of the centres of the source pulses in the reduced set will be denoted by $\rho_i^{R(n)-}$, $i = 1, ..., N_{dof}$, and the corresponding observation points on S_n^{D+} by $\rho_i^{R(n)+}$, $i = 1, ..., N_{dof}$ (Fig. 5). It is easily seen that, because of the symmetry of $\bar{\mathbf{Z}}^D$, the rows corresponding to these observation points span $\bar{\mathbf{Z}}^D$'s row range. A vast majority of these equivalent source pulses is located near the junction of D_n^- and D_n^+. The density of equivalent sources is inversely proportional to the distance to the observation region D_n^+, hence the $N_{dof} \propto \log(L)$ trend.

Given the current distribution $J_z^{S_n^{D-}}(\rho)$ on S_n^-, its field over D_n^+ can be approximated in terms of that generated by the reduced set of N_{dof} source pulses on S_n^{D-}. To this end, a reduced $N_{dof} \times N_{dof}$ matrix $\bar{\mathbf{Z}}^R$ and a reduced excitation vector $\mathbf{V}^R$ are extracted from $\bar{\mathbf{Z}}^D$ and $\mathbf{V}^D$ by selecting from the latter the N_{dof} rows and columns corresponding to the reduced sets of sources and observation points. The coefficients $\mathbf{I}^R$ of the equivalent but reduced set of sources can be computed by solving

$$\bar{\mathbf{Z}}^R\mathbf{I}^R = \mathbf{V}^R \tag{9}$$

Hence, the field in D_n^+ due to the currents residing on S_n^- can be evaluated efficiently by computing the excitation coefficients $\mathbf{I}^R$ of the reduced and equivalent source set, and by evaluating the field due to the reduced set over D_n^+.

The recursive algorithm proposed herein calls for the computation of a 'reduction matrix'. Assume that a set of N_{dof} 'old' coefficients is available, which, when associated with the reduced source set $\rho_i^{R(n-1)-}$, $i = 1, ..., N_{dof}$ on S_{n-1}^{D-}, regenerate the field radiated by a given current $J_z^{S_{n-1}^-}$ anywhere in D_{n-1}^+. We wish to compute N_{dof} 'new' coefficients, which, when associated with the reduced set of N_{dof} sources $\rho_i^{R(n)-}$, $i = 1, ..., N_{dof}$ on S_n^{D-}, regenerate the same field over D_n^+. Multiplication of the reduction matrix with the old coefficients results in the new coefficient set. From eqn. 9, it can be seen that the reduction matrix can be expressed as

$$\tilde{\bar{\mathbf{T}}} = \bar{\mathbf{Z}}^{R^{-1}}\bar{\mathbf{V}}_{\Delta x}^R \tag{10}$$

where each column of the $N_{dof} \times N_{dof}$ matrix $\bar{\mathbf{V}}_{\Delta x}^R$ expresses the field at the reduced set of observation points due to a source in the old set, i.e. $V_{\Delta xij}^R = E(\rho_i^{R(n-1)+}, p_j^{R(n-1)-})$. As Δx is constant, $\tilde{\bar{\mathbf{T}}}$ computed using eqn. 10 serves as a reduction matrix for all n.

All of the above can be reinterpreted when the source and observation domains are interchanged because of the symmetry involved. For example, the field radiated onto D_n^- by sources residing on S_n^+ can be represented by N_{dof} equivalent sources centred at $\rho_i^{R(n)+}$, $i = 1, ..., N_{dof}$. Similarly, the above defined reduction matrix $\bar{\mathbf{T}}$ can also be used to express a reduced set of sources residing on S_n^{D+} in terms of those on S_{n+1}^{D+}.

2.2 Recursive algorithm

The proposed algorithm consists of two steps, which are termed forward and backward recursion [10]. During forward recursion, transition matrices are constructed for increasingly larger subsections of the elongated structure. During backward recursion, information obtained during forward recursion is used to recover the current on the scatterer.

2.2.1 Forward recursion: During forward recursion, the algorithm iteratively constructs transition matrices $\bar{\mathbf{T}}_n$, $n = 1, 2, ..., N$, which relate the field scattered by S_n^- onto D_n^+, to the field that potentially excites S_n^-. This field consists of the field generated by the current distribution residing on S_n^+ and the incident field $E_z^{inc}(\rho)$. In view of the reduced field representation introduced in the preceding Section, the field scattered by S_n^- onto S_n^+ is expressed as

$$E_z(\rho) = \mathbf{F}_n^{-T}(\rho) \cdot \mathbf{a}_n^- \quad \forall\rho \text{ in } D_n^+ \tag{11}$$

where the N_{dof}-vector $\mathbf{F}_n^-(\rho) = [F_{ni}^-(\rho)]$ describes the fields of these sources at the observation point ρ:

$$F_{n_i}^-(\rho) = E(\rho, p_i^{R(n)-}) \quad i = 1, \ldots, N_{Dof} \tag{12}$$

and the N_{dof}-vector $\mathbf{a}_n^-$ contains the excitation coefficients associated with these sources:

$$\mathbf{a}_n^- = \left[a_{n_1}^-, a_{n_2}^-, \ldots, a_{N_{Dof}}^-\right]^T \tag{13}$$

where a superscript T denotes a transpose. The field that excites S_n^- consists of two components: (i) the field due to a set of N_{dof} equivalent sources residing on S_n^{D+} and (ii) $E_z^{inc}(\rho)$. This field is expressed as

$$E_z(\rho) = \mathbf{F}_n^{+T}(\rho) \cdot \mathbf{a}_n^+ \quad \forall\rho \text{ in } D_n^- \tag{14}$$

where the $N_{dof} + 1$-vectors $\mathbf{F}_n^+(\rho) = [F_{ni}^+(\rho)]$ and $\mathbf{a}_n^+$ are given by:

$$F_{n_i}^+(\rho) = \begin{cases} E(\rho, p_i^{R(n)+}) & i = 1, \ldots, N_{Dof} \\ E_z^{inc}(\rho) & i = N_{Dof} + 1 \end{cases} \tag{15}$$

$$\mathbf{a}_n^+ = \left[a_{n_1}^+, a_{n_2}^+, \ldots, a_{N_{Dof}}^+, 1\right]^T \tag{16}$$

The coefficient vectors $\mathbf{a}_n^+$ and $\mathbf{a}_n^-$ are related through the $N_{dof} \times (N_{dof} + 1)$ transition matrix $\overline{\mathbf{T}}_n$ as follows

$$\mathbf{a}_n^- = \overline{\mathbf{T}}_n \mathbf{a}_n^+ \tag{17}$$

Each iteration step in the forward recursion algorithm generates a transition matrix $\overline{\mathbf{T}}_{n+1}$ for the enlarged structure S_{n+1}, starting from the available transition matrix $\overline{\mathbf{T}}_n$ (with $\overline{\mathbf{T}}_0 = \overline{\mathbf{0}}$). This is achieved by enforcing the total z-directed electric field to vanish at the centre ρ_{n+1}^S of segment $n + 1$:

$$\mathbf{F}_n^{-T}(\rho_{n+1}^S)\cdot\mathbf{a}_n^- + E_{n+1}^s I_{n+1}^S + \mathbf{F}_{n+1}^{+T}(\rho_{n+1}^S)\cdot\mathbf{a}_{n+1}^+ = 0 \tag{18}$$

E_s is the self-term, which is approximated as [19]

$$E_{n+1}^s = -\frac{\eta k}{4}\left[1 - j\log\left(\frac{\gamma k w_{n+1}}{4e}\right)\right] \tag{19}$$

where γ is Euler's constant. Knowledge of $\mathbf{a}_{n+1}^+$ and I_{n+1}^S permits the computation of $\mathbf{a}_n^+$:

$$\mathbf{a}_n^+ = \overline{\mathbf{T}}^+ \mathbf{a}_{n+1}^+ + \mathbf{I}^{R+} \mathbf{I}_{n+1}^S \tag{20}$$

where $\overline{\mathbf{T}}^+$ is the $(N_{dof} + 1) \times (N_{dof} + 1)$ translation matrix describing the contribution to $\mathbf{a}_n^+$ due to all sources residing on S_{n+1}^+, as well as $E_z^{inc}(\rho)$:

$$\overline{\mathbf{T}}^+ = \begin{bmatrix} \tilde{\overline{\mathbf{T}}} & 0 \\ 0 & 1 \end{bmatrix} \tag{21}$$

and $\mathbf{I}^{R+}$ expresses source $n + 1$ on S in terms of the N_{dof} equivalent sources residing on S_n^+ using eqn. 9 as

$$\mathbf{I}^{R+} = \overline{\mathbf{Z}}^{R^{-1}} \mathbf{V}^{R+} \tag{22}$$

where

$$V_i^{R+} = E(\rho_i^{R(n)+}, p_n^S) \tag{23}$$

The incident field $E_z^{inc}(\rho)$ is not affected by the translation, which is reflected by the unit entry in the lower-right corner of $\overline{\mathbf{T}}^+$.

Substitution of eqns. 17 and 20 into eqn. 18 yields

$$\mathbf{I}_{n+1}^S = \mathbf{y}_{n+1}^T \mathbf{a}_{n+1}^+ \tag{24}$$

where $\mathbf{y}_{n+1}$ is the $(M + 1)$-vector given by

$$\mathbf{y}_{n+1}^T = -\frac{\mathbf{F}_n^{-T}(\rho_{n+1}^S)\overline{\mathbf{T}}_n\overline{\mathbf{T}}^+ + \mathbf{F}_{n+1}^{+T}(\rho_{n+1}^S)}{\mathbf{F}_n^{-T}(\rho_{n+1}^S)\overline{\mathbf{T}}_n\mathbf{I}^{R+} + E_{n+1}^s} \tag{25}$$

The vectors $\mathbf{y}_{n+1}$ are stored during forward recursion. Knowledge of $\mathbf{y}_{n+1}$ is used to obtain $\overline{\mathbf{T}}_{n+1}$ since

$$\mathbf{a}_{n+1}^- = \tilde{\overline{\mathbf{T}}}^- \mathbf{a}_n^- + \mathbf{I}^{R-} I_{n+1}^S \tag{26}$$

where $\mathbf{I}^{R-}$ is corresponds to eqn. 22 for translation to the right. Substitution of eqns. 24, 20 and 17 into eqn. 26 results in an equation for the updated transition matrix $\overline{\mathbf{T}}_{n+1}$:

$$\overline{\mathbf{T}}_{n+1} = \tilde{\overline{\mathbf{T}}}^- \overline{\mathbf{T}}_n(\overline{\mathbf{T}}^+ + \mathbf{I}^{R+}\mathbf{y}_{n+1}^T) + \mathbf{I}^{R-}\mathbf{y}_{n+1}^T \tag{27}$$

2.2.2 Backward recursion: During backward recursion, the current distribution on the strip is recovered from knowledge of $\mathbf{y}_n$, $n = 1, ..., N$. Starting from $\mathbf{a}_N^+ = (0, ..., 0, 1)^T$ and $\mathbf{y}_N$, eqn. 24 is used to compute I_N^S. I_N^S is in turn used to obtain $\mathbf{a}_{N-1}^+$ using eqn. 20. Eqns. 20 and 24 are invoked recursively to compute I_n^S, $n = N, N - 1, ..., 2, 1$. Knowledge of these expansion coefficients may be used to compute the field scattered by the strip and its RCS.

2.3 Computational complexity and TE implementation

The computational complexity of a brute-force implementation of the above algorithm is $O(N \log^3 N)$. Each iteration during forward recursion involves the multiplication of dense matrices of dimensions proportional to $\log(N)$. During forward recursion, the sequence of transition matrices $\overline{\mathbf{T}}_n$, $n = 1, ..., N$ are not stored, only the vectors $\mathbf{y}_n$, $n = 1, ..., N$ are stored; hence, the memory requirements of the algorithm grow as $O(N \log N)$. The operation count associated with the analysis of scattering from the strip for N excitations can be shown to be $O(N^2 \log N)$. The above single excitation $O(N \log^3 N)$ operation count exceeds that of Chew and Lu's spectral domain algorithm [10] for $H = 0$, by a factor of $\log N$, because the reduction matrices defined using a spectral representation of the Green function are diagonal or nearly so, whereas those in this paper (eqn. 10) are dense. However, the complexity of this solver can be reduced further through diagonalisation of the reduction operator $\overline{\mathbf{T}}$, by computing its eigenvalues and corresponding eigenvectors. These eigenvectors can equally well represent the field radiated from S_n^- on to S_n^+, as can the above described reduced basis of individual pulse sources, and the recursive solver of Section 2.2 is easily reinterpreted in terms of this new basis of eigenvectors. However, in this new basis, the reduction matrix $\overline{\mathbf{T}}$ is diagonal, which reduces the computational complexity of the algorithm to $O(N \log^2 N)$.

The computational cost of performing an RRQR decomposition on the $N^D \times N^D$ matrix $\overline{\mathbf{Z}}^D$ is $O(N^2 \log N)$, since $N^D \propto N$ and $\text{rank}(\overline{\mathbf{Z}}^D) \propto \log N$ [16]. However, knowledge of the approximate distribution of the $O(\log N)$ independent sources and observation points that characterise $\overline{\mathbf{Z}}^D$ (Fig. 6) can be used to drastically reduce this computational cost. To this end, one starts by considering a nonuniform distribution of equivalent sources that resembles the expected reduced set of Fig. 5 in the sense that the density of the sources is inversely proportional to the distance from the observation domain. Next, using this nonuniform set containing $O(\log N)$ sources, we construct the corresponding $\overline{\mathbf{Z}}^D$ matrix (which will contain $O(\log^2 N)$ elements) and perform a RRQR, to extract its linearly independent columns and rows and to estimate N_{dof}. Next, we repeat the above procedure, but using a nonuniform source set containing twice the initial number of sources. Again, we estimate N_{dof}. This procedure of doubling the number of sources is continued until N_{dof} converges, and this usually happens very quickly. This procedure has a computational cost of $O(\log^3 N)$ and serves our purpose equally well.

The above presented algorithm is easily extended to the TE case The transverse current on the strip is approximated using a set of triangular (piecewise linear) basis functions. One basis function is associated with each node on the strip, except for the two end nodes. Transverse oriented point dipoles are employed to construct a reduced representation of the fields radiated by the transverse currents on the strip. This reduced set of equivalent sources could also be constructed using axially directed magnetic sources.

3 Numerical results

Data presented in this Section were collected by implementing the above described algorithm on a SUN-SPARC10 workstation. Since standard MOM techniques require an $O(N^2)$ dense matrix fill, they are too memory intensive for analysing the problems presented in this Section. Hence, all numerical results

obtained using the proposed direct solver are compared to those obtained using an implementation of the multilevel matrix decomposition algorithm (MLMDA), an iterative fast integral equation solver for arbitrarily shaped objects [20] with $O(N \log^2 N)$ complexity per iteration.

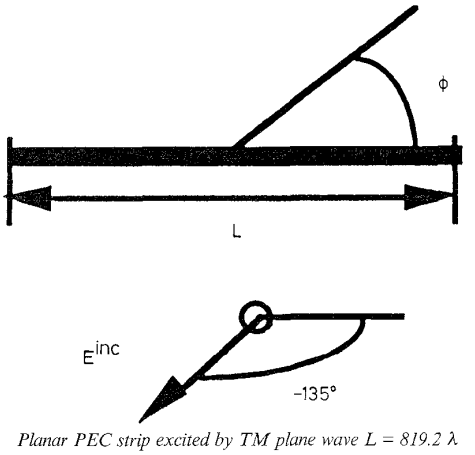

Fig. 8 *Planar PEC strip excited by TM plane wave L = 819.2 λ*

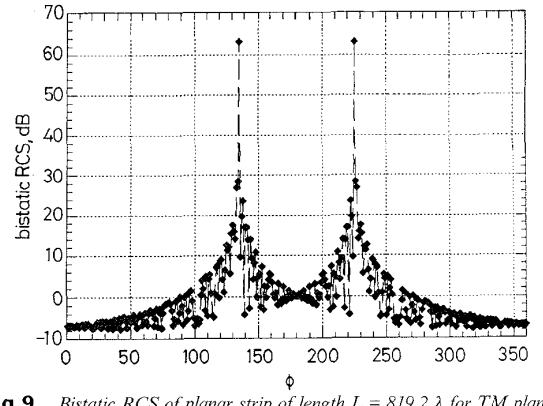

Fig. 9 *Bistatic RCS of planar strip of length L = 819.2 λ for TM plane-wave incidence*
- - - - direct solver
– ♦ – – MLMDA

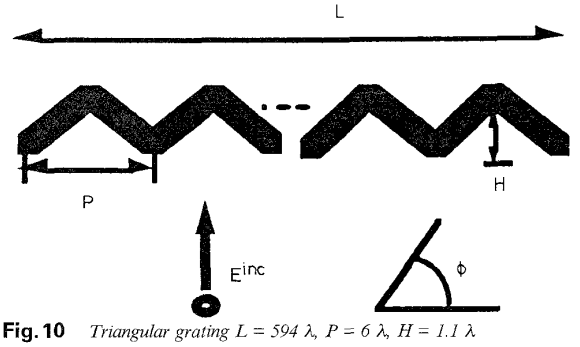

Fig. 10 *Triangular grating L = 594 λ, P = 6 λ, H = 1.1 λ*

First, consider a planar PEC strip of length L = 819.2λ, excited by a TM plane wave, as shown in Fig. 8. The current on the strip was modelled using N = 8192 pulse basis functions. Fig. 9 compares the bistatic RCSs of the strip, for an incident angle of ϕ = 135° obtained using the direct solver and the MLMDA. The RCSs obtained using both techniques agree very well.

Next, consider the finite triangular grating of length L = 594λ, periodicity P = 6λ, and height H = 1.1λ (Fig. 10). The current on the structure was modelled in terms of N = 8000 pulse basis functions. The bistatic RCS and the magnitude of the current on the grating, for a normally incident plane wave, computed using the direct solver and the MLMDA, are shown in Figs. 11 and 12, respectively. Again, perfect agreement between both results is observed. The computational complexity of the algorithm was verified by analysing larger strips and gratings (the height H of the grating was kept constant), and the results of this experiment are shown in Fig. 13. Strips and gratings modelled in terms of N = 10^5 unknowns can be analysed in approximately one and two and a half hours of CPU time, respectively. The experimentally observed computational complexity also adheres to the predicted $O(N \log^2 N)$ trend. To further verify the accuracy of the direct solver, we computed the residual error defined by

$$\varepsilon_{error} = \frac{|\bar{\mathbf{Z}}_{MOM}\mathbf{J}_{Direct} - \mathbf{V}_{MOM}|}{|\mathbf{V}_{MOM}|} \tag{28}$$

where $\bar{\mathbf{Z}}_{MOM}$ and $\mathbf{V}_{MOM}$ are the traditional MOM matrix and excitation vector, and $\mathbf{J}_{Direct}$ is the current solution vector obtained using the direct solver. Observed residual errors for various N are also shown in Fig. 13 and indicate that the algorithm is stable for all tested N. It should be noted that ε_{error} can be controlled by selecting the tolerance level in the RRQR decomposition used in constructing the reduced set of equivalent sources.

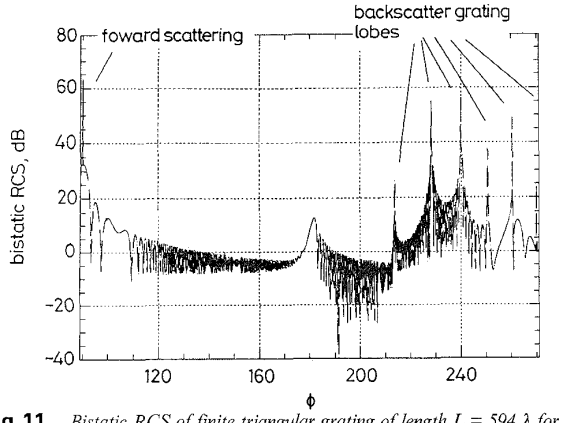

Fig. 11 *Bistatic RCS of finite triangular grating of length L = 594 λ for normal TM plane wave incidence*
Backscatter grating lobes can be observed
- - - direct solver
- - - - MLMDA

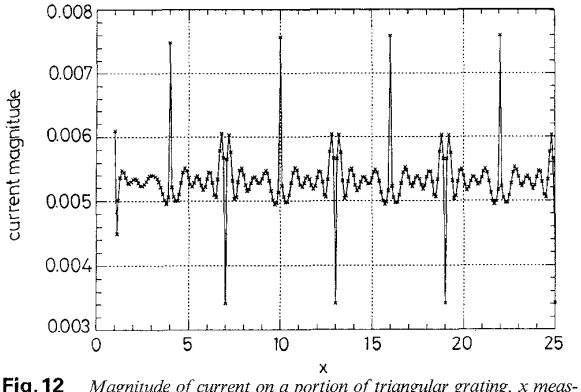

Fig. 12 *Magnitude of current on a portion of triangular grating, x measures distance to left edge of grating*
——— direct solver
× MLMDA

Scattering from the same triangular grating was investigated for oblique TE incidence ($\phi^{inc} = 45°$) The bistatic RCS obtained using the direct solver and the MLMDA are shown in Fig. 14. Finally, Fig. 15 shows the bistatic RCS of a chirped grating with a profile defined by

$$y(x) = 0.5\sin(2x^2/L) \quad -L < x < L \qquad (29)$$

for $L = 200\lambda$ ($N = 4000$). Again, the MLMDA results compare very well to those obtained using the direct solver. The latter two problems were solved in 12 and 8min of CPU time, respectively, which would obviously be impossible using traditional MOM techniques.

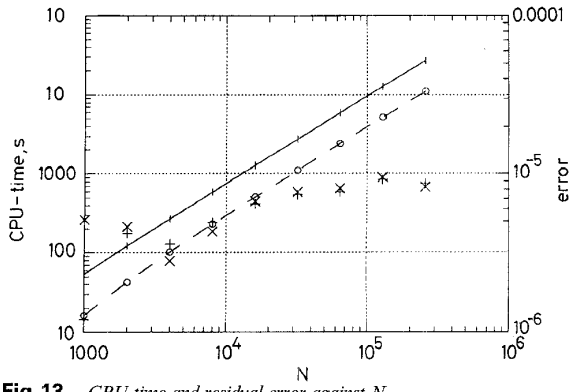

Fig. 13 *CPU time and residual error against N*
+, —○– – planar strip
×, —+— triangular grating

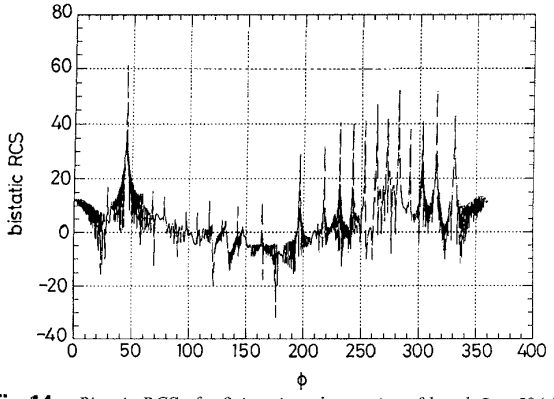

Fig. 14 *Bistatic RCS of a finite triangular grating of length L = 594 λ for TE planewave incidence ($\phi^{inc} = 45°$)*
Grating lobes can be observed
– – – direct solver
- - - - MLMDA

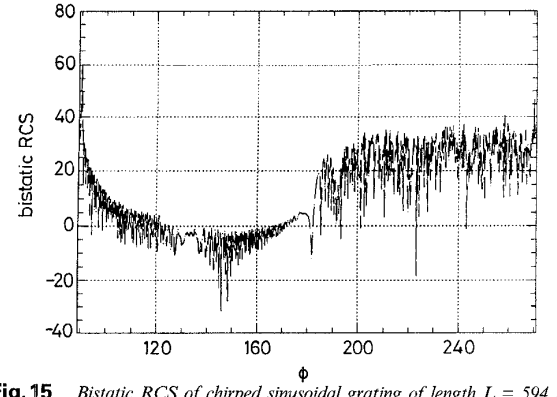

Fig. 15 *Bistatic RCS of chirped sinusoidal grating of length L = 594 λ for normal TE planewave incidence*
– – – direct solver
- - - - MLMDA

4 Conclusions

A recursive algorithm was presented for analysing TM and TE plane wave scattering from 2D elongated objects. The algorithm is based on a reduced representation of the fields that are radiated by currents residing on the elongated structure. These fields are expressed in terms of those radiated by a small, equivalent set of sources. The computational complexity and memory requirements of the algorithm are $O(N \log^2 N)$ and $O(N \log N)$, respectively. The algorithm was validated for a number of structures, such as truncated gratings. Future research will focus on extensions of the present algorithm for analysing three-dimensional structures that extend along a preferred direction, e.g. three-dimensional rough surfaces and nonplanar integrated circuits.

5 Acknowledgment

This work was supported in part by the National Science Foundation under Grant ECS-9502138.

6 References

1 ROKHLIN, V.: 'Rapid solution of integral equations of scattering in two dimensions', *J. Comput. Phys.*, 1990, **86**, pp. 414–439
2 COIFMAN, R., ROHKLIN, V., and WANDZURA, S.: 'The fast multipole method for the wave equation: a pedestrian prescription', *IEEE Antennas Propag. Mag.*, 1993, **35**, pp. 7–12
3 CANNING, F.X.: 'Transformations that produce a sparse moment method matrix', *J. Electromagn. Waves Appl.*, 1990, **4**, pp. 903–913
4 CANNING, F.X.: 'A new combined field integral equation for impedance matrix localization (IML)'. Proc. IEEE-AP/S Intl. Symp., Ann Arbor, 1993, pp. 1140–1143
5 CATEDRA, M.F., CAGO, E., and NUNO, L.: 'A numerical scheme to obtain the RCS of three-dimensional bodies of resonant size using the conjugate gradient method and the fast Fourier Transform', *IEEE Trans.*, 1989, **AP–37**, pp. 528–537
6 CHEN, C.Y., GLOVER, K.Y., SANCER, M.I., and VARVATSIS, A.D.: 'The discrete Fourier method of solving differential-integral equations in scattering theory', *IEEE Trans. Antennas Propagat.*, 1989, **37**, pp. 1032–1041
7 PAK, K., CHAN, C.H., and TSANG, L.: 'A SMFSIA method for the electromagnetic scattering from a two-dimensional (3-D scattering problem) perfectly conducting rough surface'. IEEE Antennas & Propagat. Intl. Symp., 1994, pp. 451–454
8 TSANG, L., CHAN, C.H., PAK, K., and SANGANI, H.: 'Monte-Carlo simulations of large scale composite random rough surface scattering based on the banded matrix approach', *J. Opt. Soc. Am.*, **11**
9 TSANG, L., CHAN, C.H., SANGANI, H., and ISHIMURA, A.: 'A banded matrix iterative approach to Monte Carlo simulations of large scale random rough surface scattering: TE case', *J. Electromagn. Waves Appl.*, 1993, **7**, pp. 1185–1200
10 CHEW, W.C., and LU, C.C.: 'A fast recursive algorithm to compute the wave scattering solution of a large strip', *J. Comput. Phys.*, 1993, **107**, pp. 378–387
11 BUCCI, O.M., and FRANCESCETTI, G.: 'On the spatial bandwidth of scattered fields', *IEEE Trans.*, 1987, **AP–35**, pp. 1445–1455
12 BUCCI, O.M., and FRANCESCHETTI, G.: 'On the degrees of freedom of scattered fields', *IEEE Trans.*, 1989, **AP–37**, pp. 918–926
13 FRANCIA, G.T.D.: 'Directivity, super-gain and information', *IRE Trans. Antennas Propag.*, 1956, **4**, pp. 473–478
14 FRANCIA, G.T.D.: 'Degrees of freedom of an image', *J. Opt. Soc. Am.*, 1969, **59**, pp. 779–804
15 CHEWM W.C.: 'Waves and fields in homogeneoeus media' (Van Nostrand Reinhold, New York, 1990), pp. 453–469
16 GOLUB, G.H., and LOAN, C.F.V.: 'Matrix computations' (The Johns Hopkins University Press, Baltimore, 1991), p. 642
17 BISCHOF, C.H., and HANSEN, P.C.: 'Structure preserving and rank-revealing QR-factorizations', *SIAM J. Sci. Stat. Comput.*, 1991, **12**, pp. 1332–1350
18 CHAN, T.F.: 'Rank revealing QR factorizations', *Lin. Algebr. Appl.*, 1987, **88/89**, pp. 67–82
19 HARRINGTON, R.F.: 'Field computation by moment methods' (Robert E. Krieger Publishing Company Inc., 1968), p. 229
20 MICHIELSSEN, E., and BOAG, A.: 'A multilevel matrix decomposition algorithm for analyzing scattering from large structures'. 11th Annual Review of Progress in Applied Computational Electromagnetics, Monterey, 1995, pp. 614–620